Cirrus Cloud Ice Water Content Radar Algorithm Evaluation Using an Explicit Cloud Microphysical Model

KENNETH SASSEN* AND ZHIEN WANG

Department of Meteorology, University of Utah, Salt Lake City, Utah

VITALY I. KHVOROSTYANOV

Central Aerological Observatory, Dolgoprudny, Moscow, Russia

GRAEME L. STEPHENS AND ANGELA BENNEDETTI

Department of Atmospheric Science, Colorado State University, Fort Collins, Colorado

(Manuscript received 27 August 2001, in final form 9 January 2002)

ABSTRACT

A series of cirrus cloud simulations performed using a model with explicit cloud microphysics is applied to testing ice water content retrieval algorithms based on millimeter-wave radar reflectivity measurements. The simulated ice particle size spectra over a 12-h growth/dissipation life cycle are converted to equivalent radar reflectivity factors Z_e and visible optical extinction coefficients σ, which are used as a test dataset to intercompare the results of various algorithms. This approach shows that radar Z_e-only approaches suffer from significant problems related to basic temperature-dependent cirrus cloud processes, although most algorithms work well under limited conditions (presumably similar to those of the empirical datasets from which each was derived). However, when lidar or radiometric measurements of σ or cloud optical depth are used to constrain the radar data, excellent agreement with the modeled contents can be achieved under the conditions simulated. Implications for the satellite-based active remote sensing of cirrus clouds are discussed. In addition to showing the utility of sophisticated cloud-resolving models for testing remote sensing algorithms, the results of the simulations for cloud-top temperatures of $-50°$, $-60°$, and $-70°$C illustrate some fundamental properties of cirrus clouds that are regulated by the adiabatic process.

1. Introduction

The ability of radars to remotely sense such quantities as mass content or precipitation rate via the equivalent radar reflectivity factor Z_e has been a major boon to the meteorological research community. In contrast to aircraft or precipitation gauge measurements, for example, radars offer the potential for the probing over extended regions at relatively slight cost, and space-borne deployments to obtain global coverage are promised in the near future (Stephens et al. 2002). However, the realities of radar retrievals involve major assumptions regarding the shape of the hydrometeor size distribution for each application, because radar reflectivities are dominated by essentially the largest particles present, according to the diameter D^6 law of Rayleigh scattering. Thus, crucial assumptions must be made regarding the hydrometeor size distribution to derive information concerning their lesser moments, such as mass or optical extinction, the third and second moments, respectively. It is widely known from rainfall-versus-Z_e relations, for example, that geographical and precipitation generating mechanism effects on the particle size spectra have a large impact on the relations (Battan 1973).

There are basically three ways to derive such empirical relations between Z_e and the microphysical parameter of interest: either from a scattering theory conversion of ground-based or airborne data to Z_e, a direct comparison of measured Z_e to data, or on the basis of cloud model–generated predictions of the particle size distribution (Sassen 1987; Liao and Sassen 1994). The last approach has the advantage of being able to simulate a wide range of conditions that could affect the relations and is free from associated measurement uncertainties. These uncertainties include the mismatch in remote/in situ instrument sample volumes, the size limitations in-

* Current affiliation: Geophysical Institute, University of Alaska Fairbanks, Fairbanks, Alaska.

Corresponding author: Kenneth Sassen, Geophysical Institute, University of Alaska Fairbanks, P. O. Box 757320, Fairbanks, AK 99775-7320.
E-mail: ksassen@gi.alaska.edu

herent in aircraft probes, and a variety of experimental errors. On the other hand, it is also acknowledged that cloud model predictions may suffer from numerical approach uncertainties that limit their application to describing natural clouds in detail.

In this study, we employ an approach that uses a sophisticated cirrus cloud model to generate cloud microphysical data fields that are converted to Z_e in order to evaluate in blind tests the results of various active remote sensor algorithms for inferring cirrus cloud content. A prime motivation has been to obtain the means to evaluate the plethora of radar algorithms offered in the past several years for cirrus cloud research, in order to arrive at the most suitable approach for converting global CloudSat-based radar measurements to cirrus cloud data quantities useful for climate research. The CloudSat satellite supports a 94-GHz radar and is scheduled for a 2004 deployment (Stephens et al. 2002). Elements of the cloud model used for this purpose are outlined below.

2. Cirrus cloud model

The cloud model has had a long history and has been applied to various cloud types (Khvorostyanov 1995). The nucleation, growth/evaporation, and aggregation processes are treated using the explicit modeling approach based on the kinetic equation for the particle size distribution function calculated in 30 bins between 1.0-μm and 3.5-mm radius. In other words, no bulk parameterizations often involving major assumptions are used to describe cloud growth and related radiative effects. The modeled ice crystals are grown as spheroidal particles with capacitance factors matching the behavior of cirrus particles of various habits including plates, columns, and bullet rosettes. This effectively describes the increased particle growth rates over that for the equivalent ice sphere, and radiative growth interactions are fully treated. The model used for cirrus cloud simulation is thoroughly described in Khvorostyanov and Sassen (1998a), and typical model findings are given in Khvorostyanov and Sassen (1998b). However, two important improvements have been made: an explicit evaluation of the size spectra of haze particles (after Khvorostyanov and Curry 1999) and a new description of one of the most important processes in cirrus formation, homogeneous nucleation (after Khvorostyanov and Sassen 1998c). Details of these improvements are given in Khvorostyanov and Sassen (2002).

As used here for cirrus simulation, the model contains seven basic kernels: 1) mesoscale dynamics; 2) transport of cloud condensation nuclei; 3) formation of the size spectra of deliquescent submicron aerosol (i.e., haze particles); 4) homogeneous nucleation of ice crystals; 5) cloud microphysics (kinetic equation for the crystal size spectra, and fall speeds) and thermodynamics (temperature, humidity, and supersaturation); 6) longwave radiation; and 7) solar radiation. This approach allows detailed calculations of the phase transformations and dynamics, precipitation, and the radiative characteristics of the cirrus to ensure the simulation of realistic cirrus clouds. The heterogeneous ice nucleation process, although potentially important in determining cirrus cloud content, is not treated here because of the uncertainties in specifying the activity of ice nuclei in the upper troposphere (Khvorostyanov and Sassen 2002).

The evolving model-generated ice crystal populations are expressed as size distributions of the volume-equivalent diameter D and are converted to the equivalent radar reflectivity factor ($\text{mm}^6\,\text{m}^{-3}$) from the well-known equation,

$$Z = \int N(D)D^6\,dD, \tag{1}$$

which is valid only for spheroids small enough not to violate the Rayleigh limit for backscattering, that is, for size parameters $\pi D/\lambda < 0.1$–0.4 (Liao and Sassen 1994). For larger particles a correction is applied based on Mie scattering theory. Moreover, Rayleigh–Gans backscattering for the case of randomly oriented nonspherical particles produces a slight enhancement in Z_e due to the so-called Atlas effect (Sassen and Khvorostyanov 1998). As an approximation, we have applied corrections for the effects of nonspherical particle scattering for radii larger than 30 μm using an enhancement factor between 1.0 and 1.4, which depends linearly on radius within the range of 30–3500 μm (see Matrosov 1992; Atlas et al. 1995).

Similarly, the visible extinction coefficient σ is calculated from the second moment of the size spectra using the mass-equivalent solid ice sphere, which is then simply increased by 20% to account for the effects of ice density and typical nonspherical particle shape effects, according to recent theoretical analyses (Fu 1996; Yang et al. 2000).

3. Cirrus cloud model simulations, and discussion

For the application of interest here, the model was run in a 2D mode with subsequent averaging over the 4.8-km-wide horizontal domain to obtain vertical profiles of cloud content at 20-min intervals of cloud development. The computational resolutions in the domain are 200-m height and 150-m distance, which are adequate to capture the main features of cirrus cloud content for our purposes. The simulations are initiated on the basis of a generic midlatitude-type sounding with a 1.5-km-thick ice-saturated layer overlying a thick subsaturated layer, displaying the stable thermodynamic profile distributed within Working Group 2 of the Global Energy and Water Cycle Experiment (GEWEX) Cloud System Study (Starr 1997). In order to assess any temperature dependencies in the modeled and retrieved cirrus findings, the sounding profile was adjusted such that at about the same height–pressure, cloud-top temperatures occur at about $-50°$, $-60°$, and $-70°$C. The initial potential temperature profile allows for stable ascent,

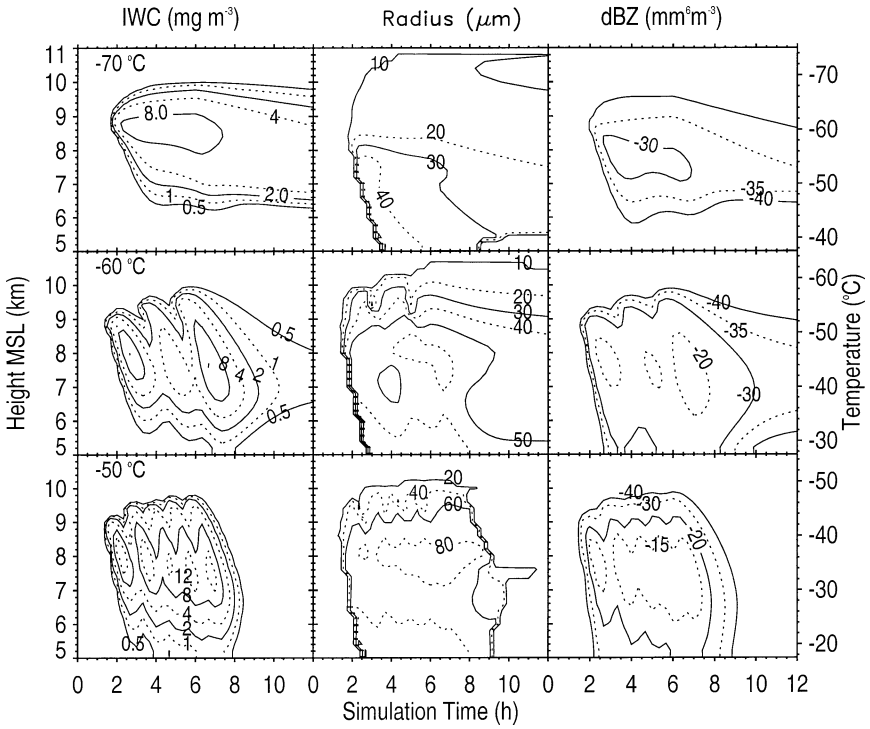

FIG. 1. Model-predicted cirrus cloud ice water content, mean equivalent radius, and radar reflective factor fields over 12-h cloud growth and dissipation cycles for the three cloud-top temperatures indicated at top left of each row. Both height and initial temperature scales are given.

which is modeled as a constant (slow synoptic-scale) uplift of 3 cm s^{-1} for the first 6-h of each simulation. After this initial growth period, the ascent rate is reduced to zero in order to produce cirrus cloud content changes associated with cloud decay.

Figure 1 provides, for each cloud-top temperature run, height-versus-simulated-time displays of ice water content (IWC), crystal mean equivalent radius [i.e., the size of a mass equivalent ice sphere as in Khvorostyanov and Sassen (1998a)], and equivalent radar reflectivity factor in $\mathrm{dBZ} = 10 \log Z_e$ computed from Eq. (1). Figure 2 shows the evolution with time of the corresponding ice water path (IWP, the vertical integral of IWC) as solid lines (see below for other curves). Last, examples of ice crystal equivalent radius size spectra are given in Figs. 3 a–c for the three cloud-top temperature simulations, at altitudes ranging from near cloud base (6 km) to near cloud top (9 km). These spectra correspond to the mature cloud conditions present at 6-h of simulated time.

Before moving on to testing the radar cloud property retrieval algorithms, it is useful to consider the basic model findings, concerning in particular the temperature dependencies in cirrus properties. This knowledge has implications for understanding this radar algorithm intercomparison project, as well as shedding light on the fundamental behaviors of midlatitude cirrus. That ambient temperature has a great deal of influence on cirrus clouds is naturally a consequence of the adiabatic process in cloud particle growth rates. The growth, or evaporation, rate of hydrometeors decreases considerably with decreasing temperature.

Quite noticeable features of the simulated cirrus are how they are generated and their lifetimes after forced ascent ceases. As revealed especially by the IWC fields (Fig. 1, left), cirrus generation is accomplished via a succession of particle generating ''pulses'' that arise near cloud top and produce fallstreaks that increase the cloud depth, until particle evaporation occurs in subsaturated air below. Interestingly, the number of generating pulses decreases from 6, to 3, to 1 as the cloud-top temperature decreases from $-50°$, to $-60°$, to $-70°$C; the maximum IWC and mean equivalent radius in the fallstreaks also correspondingly decrease. These pulses may be analogous to the features described in the cirrus parcel model experiments of Sassen and Dodd (1989). It was shown in that study that after sufficient supersaturation was reached to initiate ice crystal nucleation homogeneously in a uniform updraft, the supersaturation decreased from ice crystal growth and could not regain the level needed for additional nucleation until particle fallout occurred. The pulselike action of IWC generation in Fig. 1 appears to be controlled by similar cycles in the ice supersaturation fields (not shown), as has been discussed recently on the basis of model and radar findings in Khvorostyanov et al. (2001).

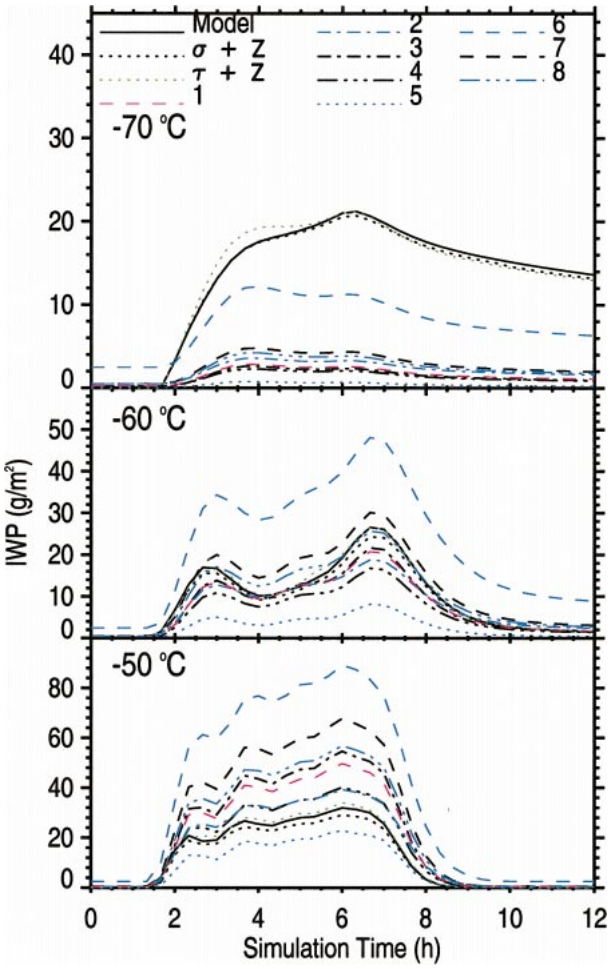

FIG. 2. Comparison of radar Z_e-only (labeled 1 through 8, see Table 1) and two hybrid algorithm estimations of ice water path with the predictions for the three cloud-top temperature model runs (solid lines).

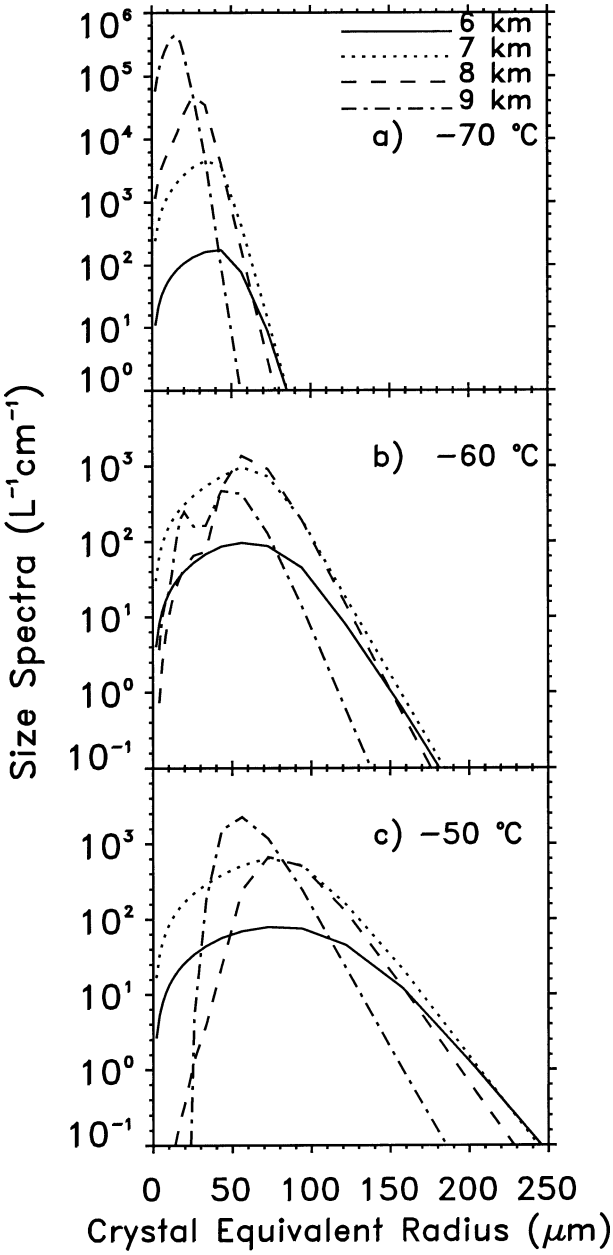

FIG. 3. Examples of domain-averaged ice crystal equivalent radius size spectra for cloud-top temperatures of (a) −70°, (b) −60°, and (c) −50°C, at altitudes ranging from near cloud base (6 km) to near cloud top (9 km). These spectra represent the mature cloud conditions after 6 h of simulated growth.

Thus, temperature governs the number of generating pulses and the cirrus cloud lifetimes in the model: more rapid growth at warmer temperatures is also associated with the faster cloud decay due to the higher fallout and evaporation rates.

The IWP traces in Fig. 2 and the crystal size spectra plots in Fig. 3 also reveal the action of temperature-dependent process in cirrus cloud formation. Because the spectra were chosen arbitrarily at 6 h of model growth time, the individual domain-averaged spectra in Fig. 3 are influenced by local variations in the positions of particle generation areas and fallstreaks. Note the general effects of particle evaporation near the cloud bases and the small particle peaks in the bimodal spectra of Fig. 3b near cloud top, which captured at this time a particle generating zone. Nonetheless, it is clear that with decreasing temperature the size distribution widths decrease significantly, as does IWP.

The combined action of these microphysical processes produces, in terms of the sixth moment of the local size spectra, the fields of Z_e given at the right of Fig. 1, where a large dynamic range (dBZ) is predicted by the model over a 20°C cloud-top temperature range. Since the maximum IWP values decrease only from 31 to 21 g m^{-2} over this range of temperature, it is apparent that changes in the particle size spectra due to temperature-induced variations in the rates of nucleation, growth/evaporation, and aggregation are mainly responsible for the great range in Z_e.

TABLE 1. Empirical relationships between IWC and millimeter-wave radar Z_e considered in this study. IWC and Z_e: g m^{-3} and mm^6 m^{-3}, respectively.

No.	Relationship	Size distribution source	Reference
1*	$IWC = 0.12Z_e^{0.696}$	Ground, precipitating ice crystals	Sassen (1987)
2	$IWC = 0.064Z_e^{0.58}$	Aircraft samples, cirrus	Atlas et al. (1995)
3	$IWC = 0.153Z_e^{0.74}$	Aircraft samples, cirrus	Brown et al. (1995)
4	$IWC = 0.097Z_e^{0.696}$	Modeled size spectra	Schneider and Stephens (1995)
5*	$IWC = 0.086Z_e^{0.83}$	Ground, precipitating ice crystals	Sassen and Liao (1996)
6	$IWC = 0.104Z_e^{0.483}$	Modeled size spectra	Aydin and Tang (1997)
7	$IWC = 0.137Z_e^{0.643}$	Aircraft samples, cirrus	Liu and Illingworth (2000)
8	$IWC = 0.11Z_e^{0.63}$	Average of retrieved results	S. Matrosov (2001, personal communication)

* Relations converted from Z_i appropriate for ice to Z_e (see Sassen 1987).

4. Remote sensor algorithm testing

a. Radar Z_e-only algorithms

The dBZ time–height displays at the right of Fig. 1 provide a test dataset to evaluate the predictions of IWC and IWP from available Z_e–IWC relations. That is, the predicted Z_e are used to derive cirrus cloud composition using various empirically based algorithms, which can then be tested against the model–truth values. Although not exhaustive, Table 1 compiles the algorithms for millimeter-wave radar and cirrus clouds considered in this study—additional algorithms based on similar approaches to these have been omitted for the sake of clarity in the intercomparison figures. Also listed in Table 1 is the general method used in deriving the retrieval algorithm. Figure 4 shows graphically the forms of the various relationships between Z_e and IWC.

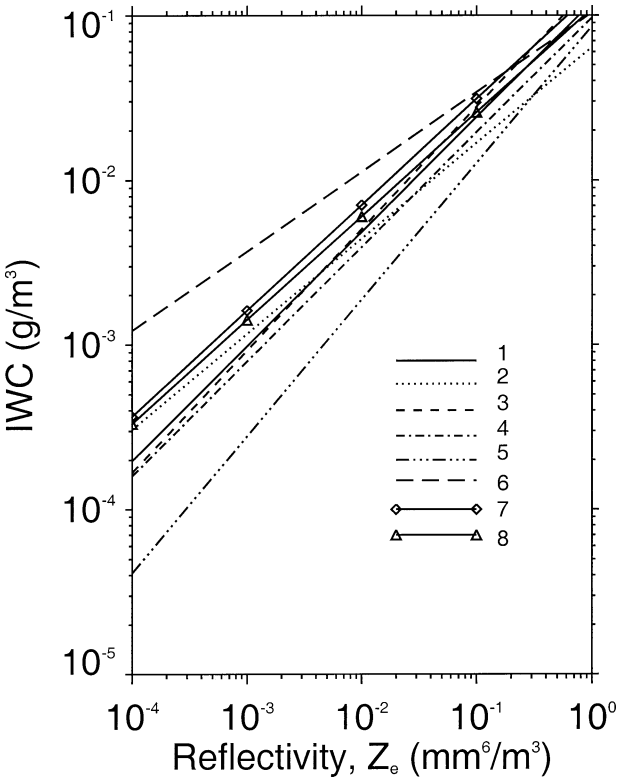

FIG. 4. Comparison of the results of the eight radar Z_e vs IWC algorithms tested (see Table 1 for numerical key).

The intercomparison results in terms of IWP are shown in Fig. 2 as compared with the three model-truth predictions (see the key in Table 1 for identifying the number of each algorithm). It is clear that the eight radar algorithms all have great difficulties in converting the modeled Z_e to IWP under the range of cirrus cloud conditions simulated. Although at the −60°C cloud-top temperature most of the algorithm results cluster around the (solid) model curve, most algorithms significantly overestimate IWP at −50°C and all significantly underestimate IWP at −70°C. In other words, while the model has generated cloud compositions that can generally be applied favorably to the algorithms at a −60°C cloud-top temperature, the compositions predicted by the same cloud model appear to disclose significant errors at other temperatures.

Instead of comparing the vertically integrated IWP values, Fig. 5 shows the differences between the vertically resolved algorithm and model IWC results. Here we use the (most favorable) −60°C cloud-top temperature modeled IWC (shown at top left) and then provide for each algorithm the differences in local IWC (mg m^{-3}). Algorithms 5 and 6, which display the poorest IWP agreements (Fig. 2) at this temperature, not surprisingly consistently underestimate and overestimate IWC in nearly all portions of the model domain, respectively. However, the remaining six algorithms have produced similar patterns with respect to their differences with the model values. We see that IWC is (a) underestimated in the three generating pulses having the highest masses, particularly (i.e., percentage-wise) near the heads of the pulses where new particle generation occurs; and (b) overestimated in evaporating portions of the clouds, where small particles are being preferentially removed and the effects of aggregation are the most pronounced (see Fig. 3b). The fact that these algorithms have produced IWP values that are similar to those modeled can now be seen to be a consequence of partially canceling out the negative and positive errors in the predicted IWC fields. It appears that, in relation

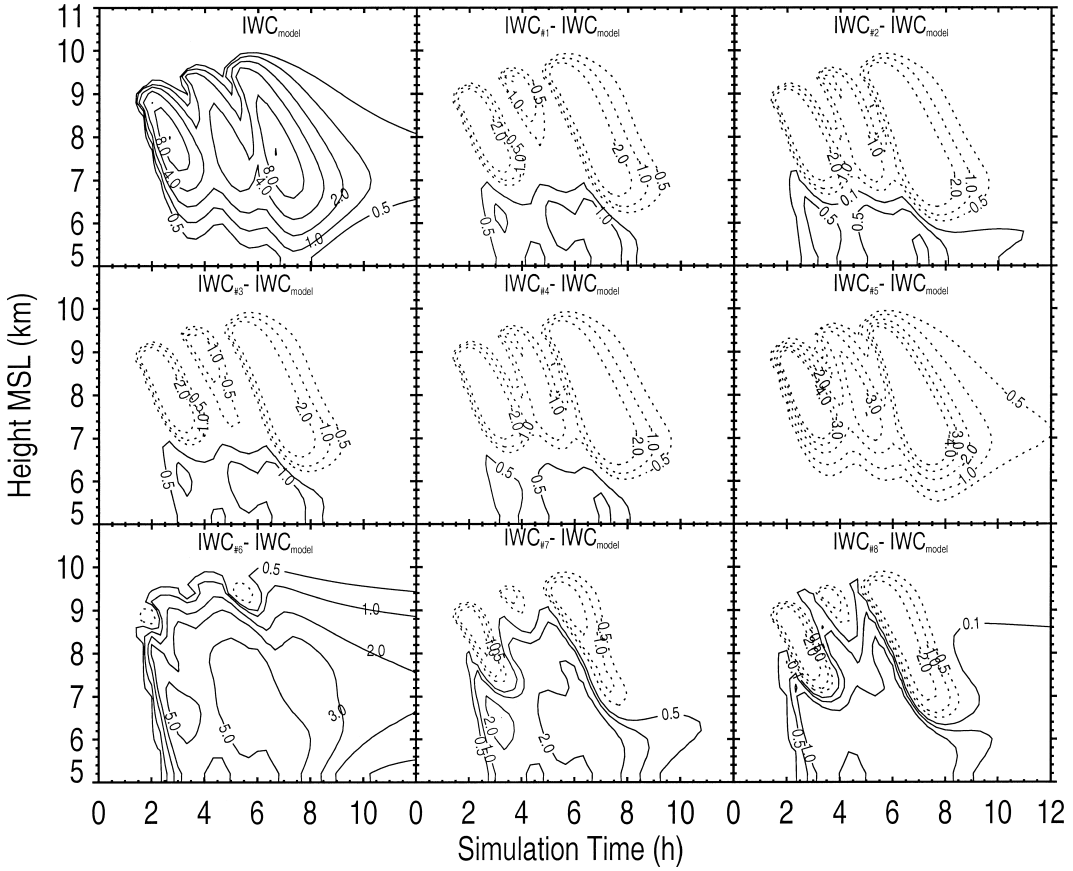

FIG. 5. Comparison of the differences between the −60°C model IWC field (top left) with each of the eight algorithms (numbered according to Table 1), in terms of the under- (dotted) and overestimation (solid) of IWC contoured in milligrams per cubic meter.

to the cloud model predictions of cirrus microstructure and Z_e, the failings of the algorithms are related to the effects of various cloud microphysical processes that affect the particle size spectra.

b. Radar Z_e plus visible optical extinction

An alternative approach to the radar Z_e-only algorithm involves the use of supplemental information from additional remote sensing instruments. As reviewed in Sassen and Mace (2002), such methods rely on coordinated probing using radiometers or lidars to constrain and improve the radar retrievals. In this study, we also test two new hybrid approaches combining the measurement of Z_e and visible cloud optical depth τ, or height-resolved σ. The latter approach has the advantage of allowing the direct retrieval of vertical profiles of IWC and the mean particle size when using, say, a suitable Raman or high-spectral-resolution lidar. These methods are part of a growing interest in applying multiple remote sensor measurements to deriving cloud contents, and can be expected to become increasingly sophisticated with time.

Method A is based on constraining the radar Z_e analysis with the knowledge of τ. The retrieval approach is adapted from Austin and Stephens (2001), based on work by Rodgers (1990) and Marks and Rodgers (1993). It is formulated in the context of estimation theory, which allows for the inclusion of a priori information, and provides a quantitative estimate of the uncertainty in the retrieved quantities and the relative influence of the measurements and a priori data on the retrieved products. Austin and Stephens (2001) describe an optimal-estimation retrieval of stratus cloud microphysical parameters, which assumes a lognormal cloud droplet size distribution and uses radar measurements and cloud optical depth information. Here it is applied to cirrus clouds. The ice crystals are assumed to be distributed according to a modified gamma size distribution (Stephens et al. 1990) defined by the total number concentration, the characteristic diameter, and the distribution width. In principle, all the distribution parameters are functions of the vertical coordinate, and $3n$ independent measurements, with n number of cloud levels, would be needed to fully retrieve the parameter profiles. In practice, we have only a radar reflectivity profile of n measurements and a column cloud optical depth, for a total of $(n + 1)$ measurements. The assumptions made

to reduce the number of retrieved quantities are that the distribution width has a fixed value of 2, and that the number concentration is also constant with height. A layer-average value for the number concentration is then retrieved, along with the characteristic diameter profile. IWC is computed from these two quantities, assuming spherical particles and a bulk ice density of 0.92 g m^{-3}. The radar forward model is based on the Rayleigh approximation, assumed valid for W-band radar. To account for non-Rayleigh effects for larger-sized crystals, a correction based on exact Mie calculations for Z_e is implemented. More details on the retrieval can be found in Benedetti and Stephens (2001).

Method B relies on combining radar Z_e and lidar σ measurements to estimate vertical profiles of cirrus cloud IWC and general effective size D_{ge}. Based on the treatment of the radiative properties of cirrus clouds developed by Fu (1996), the visible extinction coefficient (σ) can be parameterized as

$$\sigma = \mathrm{IWC}(a_0 + a_1/D_{ge}), \tag{2}$$

where a_0 and a_1 are constants at visible wavelengths. Using the same assumptions about ice crystal shape as in Fu (1996), and further assuming that the Rayleigh approximation is valid and the radar reflectivity of hexagonal ice crystals is equal to that of equivalent volume ice spheres (Liao and Sassen 1994), water-equivalent Z_e can be parameterized approximately as,

$$Z_e = C'(\mathrm{IWC}/\rho_i)D_{ge}^b, \tag{3}$$

where C' and b are constants assuming a modified gamma size distribution. Then it is straightforward to retrieve IWC and D_{ge} profiles according to this simple parameterization. Details of this approach are given in Wang and Sassen (2002).

The results of applying these hybrid algorithms to the model-generated Z_e and σ are shown in terms of IWP in Fig. 2 as the curves labeled $\tau + Z$ (method A) and $\sigma + Z$ (method B). Unlike the significant temperature-dependent errors seen in the Z_e-only algorithms, these methods generate close agreement with the model values for each run. Using the ability of method B to directly retrieve range-resolved IWC, we provide in Fig. 6 comparisons between the model and algorithm results (as in Fig. 5). Generally, only a small negative difference from the model IWC is found. (The only positive error occurs at the head of the third generating pulse in a small area.) The relatively small underestimation of IWC, in comparison with the Z_e-only results given in Fig. 5, results from the fact that the increase in radar backscattering for nonspherical particles was not taken into account in the method B analysis, and the method for treating hollow ice particles is approximate.

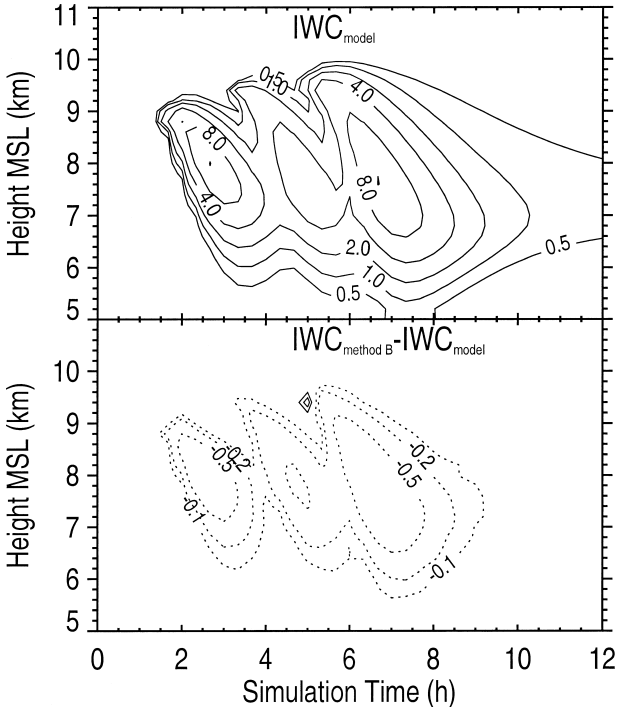

FIG. 6. As in Fig. 5 except showing the differences between the IWC results from the model (top) and the method B ($\sigma + Z_e$) hybrid algorithm.

5. Conclusions

Although it is arguable whether the cloud particle size distributions generated by the model would be *verified* by available in situ probes under environmental conditions closely matching those of these idealized cases, we stress that the model predictions are *realistic* in that they take explicitly into consideration the fundamental cirrus cloud microphysical processes. Regardless of how accurately dynamical/radiative effects on cloud growth are treated in this model, rigorously taking into account the processes of homogeneous ice crystal nucleation, competitive growth and evaporation, and aggregation produces results that reflect a large range of cirrus cloud microphysical conditions. Thus, the ensuing evolution of the particle size spectra with altitude and time, with growth and dissipation, and as a function of cloud-top temperature, spans a wide range of conditions over the life cycle of typical midlatitude cirrus clouds. In testing remote sensing algorithms for deriving cloud contents, one must subject the relations to such variable conditions to fully evaluate them, and cloud-resolving model predictions provide a comprehensive approach free from in situ instrumental effects.

We have found that available radar Z_e–IWC relations are incapable of accounting for the variations in cirrus cloud content that the model predicts are a function of cloud-top temperature. As also suggested by Atlas et al. (1995), it is apparent that simple Z_e–IWC relations are inadequate because of fundamental temperature dependencies in cloud content. Over the $-50°$ to $-70°$C range of cloud-top temperatures simulated, the maximum IWP decreases from 31 to 21 g m^{-2}, but the corresponding

changes in the particle size distributions were much more profound in their influence on Z_e and the algorithm results. It is particularly the increase in the large-particle tail of the size spectra with increasing temperature (Fig. 3) that is undoubtedly responsible for affecting the algorithm results. Although for the −60°C cloud-top case most of the Z_e-only IWP results are reasonably close to those that are model generated, all these algorithms underestimate IWP and most overestimate IWP at −70°C and −50°C, respectively. Moreover, examining where in the clouds the errors occur (Fig. 4) reveals what microphysical processes are likely responsible: it is in regions of new particle generation and evaporation that the algorithms appear to fail most drastically.

We interpret these findings in the following way. The eight representative algorithms tested are derived empirically from various field datasets. Aside from possible errors in the details of each approach (i.e., inappropriate scattering theory or probe measurement uncertainties), we speculate that the rather consistent temperature-based differences with the model findings may reflect the temperature bias of the in situ ice crystal samples used in deriving each relation. In other words, it appears that most measurements were collected within cirrus having a −60°C, or somewhat warmer, cloud-top temperature, although possible inaccuracies in the model results may have influenced this finding. Interestingly, according to the 10-yr midlatitude cirrus sample described in Sassen and Campbell (2001), synoptic (i.e., excluding anvil) cirrus have a similar −55.7°C mean cloud-top temperature.

It remains to be seen whether an effective temperature-dependence term can be incorporated into Z_e–IWC relations to increase their usefulness (Liu and Illingworth 2000), particularly because ambient temperature *alone* may not be sufficient information. Here, we refer to the additional effect that the height from cloud top has on microphysics at a given temperature. For example, it can be appreciated from Fig. 1 that the cloud compositions at, say, the −45°C level are quite different in the three model runs, where that level represents dissipating, mature, and generating stages over the −70° to −50°C cloud-top temperature range. The approach suggested in Atlas et al. (1995) of using a Z_e–IWC relation that includes an effective particle diameter term could be pursued in further research if mean particle size can be shown to be a function of height from cloud top for a given cloud-top temperature. As in the current study, this endeavor may be facilitated through the use of sophisticated cloud model findings.

Last, we point out that the two other methods tested, which are constrained by visible cloud optical depth or range-resolved extinction coefficients, provide excellent agreement with the IWP model results regardless of temperature, thus avoiding current radar Z_e-only uncertainties. Therefore, it is highly worthwhile to pursue combined lidar and/or radiometric approaches to increase the utility of radar for sensing ice cloud microphysical content. Several promising methods using combined radar or lidar and infrared radiometer measurements are reviewed in Sassen and Mace (2002). Described in Wang and Sassen (2002) is a method combining Raman lidar (for direct cloud σ measurement) with millimeter-wave radar to derive IWC and effective size, which is essentially the same method as used here. Sensitive lidars also have the advantage of probing cirrus clouds containing particles that are too small to be detected by current radars. As for the radar/radiometer approach, this appears particularly promising in the case of upcoming space-borne radar applications, where the 94-GHz CloudSat radar reflectivities can be combined with τ estimates from satellite radiometers, provided the passive methods provide sufficiently accurate data over the required range. Alternatively, combined CloudSat millimeter-wave radar and Cloud-Aerosol Lidar and Infrared Pathfinder Satellite Observations (CALIPSO) visible lidar backscattering profiles can lead to improved retrievals of cirrus cloud content. It is currently necessary to constrain radar reflectivity measurements by coincident measurements in the optical domain, which are inherently more sensitive to those spectral moments controlling the scattering of light and the mass of the scatterers.

Acknowledgments. This research has been funded by DOE Grant DEFG0394ER61747 from the Atmospheric Radiation Measurement program, and NASA Grant NAS-7-1407 from the CloudSat program.

REFERENCES

Atlas, D., S. Y. Matrosov, A. J. Heymsfield, M.-D. Chou, and D. B. Wolf, 1995: Radar and radiation properties of ice clouds. *J. Appl. Meteor.*, **34,** 2329–2345.

Austin, R. T., and G. L. Stephens, 2001: Retrieval of stratus cloud microphysical parameters using millimetric radar and visible optical depth in preparation for CloudSat. Part I: Algorithm formulation. *J. Geophys. Res.*, **106,** 28 237–28 242.

Aydin, K., and C. Tang, 1997: Relationships between IWC and polarimetric radar measurements at 94 and 220 GHz for hexagonal columns and plates. *J. Atmos. Oceanic Technol.*, **14,** 1055–1063.

Battan, L. J., 1973: *Radar Observation of the Atmosphere.* University of Chicago Press, 324 pp.

Benedetti, A., and G. L. Stephens, 2001: Characterization of model errors in cirrus simulations from a cloud resolving model for application in ice water content retrievals. *Atmos. Res.*, **59–60,** 393–417.

Brown, P. R., A. J. Illingworth, A. J. Heymsfield, G. M. McFarquhar, K. A. Browning, and M. Gosset, 1995: The role of spaceborne millimeter-wave radar in the global monitoring of ice cloud. *J. Appl. Meteor.*, **34,** 2346–2366.

Fu, Q., 1996: An accurate parameterization of the solar radiative properties of cirrus clouds for climate models. *J. Climate,* **9,** 2058–2082.

Khvorostyanov, V. I., 1995: Mesoscale processes of cloud formation, cloud-radiation interaction and their modeling with explicit cloud microphysics. *Atmos. Res.*, **39,** 1–67.

——, and K. Sassen, 1998a: Cirrus cloud simulation using explicit microphysics and radiation. Part I: Model description. *J. Atmos. Sci.*, **55,** 1808–1821.

——, and ——, 1998b: Cirrus cloud simulation using explicit mi-

crophysics and radiation. Part II: Microphysics, vapor and ice mass budgets, and optical and radiative properties. *J. Atmos. Sci.,* **55,** 1822–1845.

——, and ——, 1998c: Towards the theory of homogeneous nucleation and its parameterization for cloud models. *Geophys. Res. Lett.,* **25,** 3155–3158.

——, and J. A. Curry, 1999: A simple analytical model of aerosol properties with account for hygroscopic growth. Part I: Equilibrium size spectra and CCN activity spectra. *J. Geophys. Res.,* **104** (D2), 2163–2174.

——, and K. Sassen, 2002: Microphysical processes in cirrus and their impact on radiation: A mesoscale modeling perspective. *Cirrus,* D. Lynch, et al., Eds., Oxford University Press, 397–432.

——, J. A. Curry, J. O. Pinto, M. Shupe, B. A. Baker, and K. Sassen, 2001: Modeling with explicit spectral water and ice microphysics of a two-layer cloud system of altostratus and cirrus observed during the FIRE Arctic Clouds Experiment. *J. Geophys. Res.,* **106,** 15 099–15 112.

Liao, L., and K. Sassen, 1994: Investigation of relationships between K_a-band radar reflectivity and ice and liquid water contents. *Atmos. Res.,* **34,** 231–248.

Liu, C., and A. J. Illingworth, 2000: Toward more accurate retrievals of ice water content from radar measurements of clouds. *J. Appl. Meteor.,* **39,** 1130–1146.

Marks, C. J., and C. D. Rodgers, 1993: A retrieval method for atmospheric composition from limb emission measurements. *J. Geophys. Res.,* **98,** 14 939–14 953.

Matrosov, S. Y., 1992: Radar reflectivity in snowfall. *IEEE Trans. Geosci. Remote Sens.,* **30,** 454–461.

Rodgers, C. D., 1990: Characterization and error analysis of profiles retrieved from remote sounding measurements. *J. Geophys. Res.,* **95,** 5587–5595.

Sassen, K., 1987: Ice cloud content from radar reflectivity. *J. Climate Appl. Meteor.,* **26,** 1050–1053.

——, and G. C. Dodd, 1989: Haze particle nucleation simulations in cirrus clouds, and applications for numerical and lidar studies. *J. Atmos. Sci.,* **46,** 3005–3014.

——, and L. Liao, 1996: Estimation of cloud content by W-band radar. *J. Appl. Meteor.,* **35,** 932–938.

——, and V. I. Khvorostyanov, 1998: Radar probing of cirrus and contrails: Insights from 2D model simulations. *Geophys. Res. Lett.,* **25,** 975–978.

——, and J. R. Campbell, 2001: A midlatitude cirrus cloud climatology from the Facility for Atmospheric Remote Sensing. Part I: Macrophysical and synoptic properties. *J. Atmos. Sci.,* **58,** 481–496.

——, and G. G. Mace, 2002: Ground based remote sensing of cirrus clouds. *Cirrus,* D. Lynch, et al., Eds., Oxford University Press, 168–196.

Schneider, T. L., and G. L. Stephens, 1995: Theoretical aspects of modeling backscattering by cirrus particles at millimeter wavelengths. *J. Atmos. Sci.,* **52,** 4367–4385.

Starr, D. O'C., cited 1997: Cirrus Clouds Models Intercomparison Project. [Available online at http://eos913.gsfc.nasa.gov/gcsswg2.]

Stephens, G. L., S.-C. Tsay, P. W. Stackhouse, and P. J. Flatau, 1990: The relevance of the microphysical and radiative properties of cirrus clouds to climate and climatic feedback. *J. Atmos. Sci.,* **47,** 1742–1753.

——, and Coauthors, 2002: The CloudSat mission and the EOS constellation: A new dimension of space-based observations of clouds and precipitation. *Bull. Amer. Meteor. Soc.,* in press.

Wang, Z., and K. Sassen, 2002: Cirrus cloud microphysical property retrieval using lidar and radar measurements. Part I: Algorithm description and comparison with in situ data. *J. Appl. Meteor.,* **41,** 218–229.

Yang, P., K. N. Liou, K. Wyser, and D. Mitchell, 2000: Parameterization of the scattering and absorption properties of individual ice crystals. *J. Geophys. Res.,* **105,** 4699–4718.